HIERARCHICAL DUAL-LOOP SPEED CONTROL FOR A HELICOPTER.

Giulia Bertolani, giulia.bertolani2@unibo.it, University of Bologna, (Italy)
Andrea D. Ryals, andrea.ryals@phd.unipi.it, University of Pisa, (Italy)
Emanuele L. de Angelis, emanuele.deangelis4@unibo.it, University of Bologna, (Italy)
Fabrizio Giulietti, fabrizio.giulietti@unibo.it, University of Bologna, (Italy)

Abstract

In this article, the authors explore ways to optimize helicopter performance by utilizing various control techniques that cater to different operational requirements and flight conditions. By combining these techniques in a hierarchical structure, helicopter engineers and researchers can enhance the aircraft's versatility and overall effectiveness. The work focuses on integrating different control strategies and evaluating their performance during various maneuvers. The inner loop control for pitch, roll, and yaw uses a cascaded P-PI controller, while the outer loop control for horizontal and lateral speed employs a Sliding Mode Controller to provide pitch and roll references for the inner loop. For vertical speed control, $\mathcal{L}_1$ adaptive controller has been implemented. This paper provides valuable insights into the practical implementation and performance analysis of these integrated control strategies, showcasing their potential significance in addressing the diverse and demanding environments encountered during helicopter missions.

1. INTRODUCTION

Helicopters present unique control challenges due to their inherent complexity and nonlinearity, making them sensitive to changes in aerodynamics, uncertainties, and external factors such as wind gusts or turbulence.[1],[2],[3] A robust control system is indeed necessary to fly helicopters maintaining stability, accurately tracking desired flight trajectories and waypoints, rejecting external disturbances, and adapting to changes in the helicopter's dynamics. Various robust control techniques have been applied to helicopters. H_∞control, a robust control method, minimizes the impact of uncertainties and disturbances on the helicopter's performance by formulating the control problem as an optimization task.[4],[5] The Model Predictive Control (MPC) based approach demonstrated good closed-loop performance for the helicopter in the presence of disturbances. Nonetheless, it is essential to consider the added computational expenses and resource requirements associated with implementing MPC.[6],[7] Adaptive control techniques continuously adjust the control parameters based on real-time system information. This adaptability enables the control system to handle changes in the helicopter's dynamics, making it more resilient and robust in various operational scenarios.[8],[9],[10] A promising technique for helicopter control is Sliding Mode Control (SMC). SMC is a robust control strategy used in various engineering applications to regulate the behavior of dynamic systems. It has gained popularity due to its ability to handle uncertainties and disturbances in control systems. Sliding mode control has proved its ability to control a helicopter in previous works effectively.[11],[12],[13]

Various control techniques have been proven effective in optimizing helicopter performance in different flight conditions and operational needs. These techniques excel in specific flight regimes or address particular challenges. Combining them allows helicopter engineers and researchers to leverage their strengths and enhance the versatility and overall effectiveness of the aircraft. This is particularly important given the diverse environments and mission scenarios in which helicopters are utilized.

The paper's primary focus is on integrating various control strategies into a hierarchical structure and analyzing their performance in different maneuvers. The pitch, roll, and yaw inner loop control uses a cascaded P-PI controller, while the outer loop control for horizontal and lateral speed relies on a Sliding Mode Controller (SMC) that provides pitch and roll references for the inner loop. The $\mathcal{L}_1$ adaptive controller handles the vertical speed control.

The paper introduces the main physical model of the helicopter used in the simulation, a BO105, in section 2. Then the main theory behind the SMC control is depicted in section 3. The main concept behind the $\mathcal{L}_1$ is not presented in this paper due to the standard implementation of the controller and the works in references.[14],[9],[10] Section 4 describes the control architecture with a particular focus on the implementation of the SMC controller. Section 5 describes the simulation results of the proposed combined hierarchical architecture in three test maneuvers: bob-down bob-up, slalom, and a rectangular closed loop maneuver. Finally Section 6 describes the final consideration of this work.

2. HELICOPTER MATHEMATICAL MODEL

In this section the complete nonlinear mathematical model of the helicopter is presented.

2.1. Reference frames and coordinate transformation

Four reference frames are introduced, as in Fig.1, 2, 3 namely: NED, Hub-Wind, Hub-Body and Body RF.

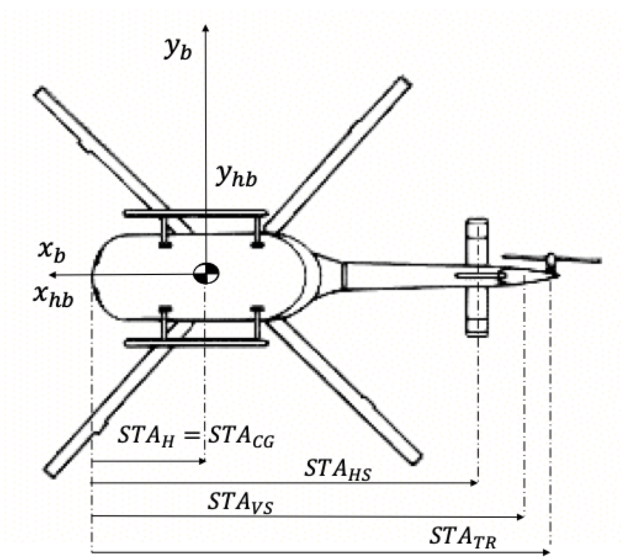

Figure 1: Helicopter xy view

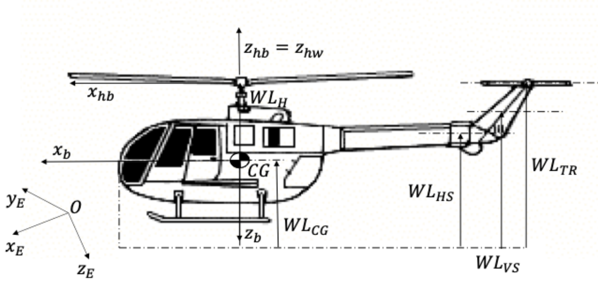

Figure 2: Helicopter xz view

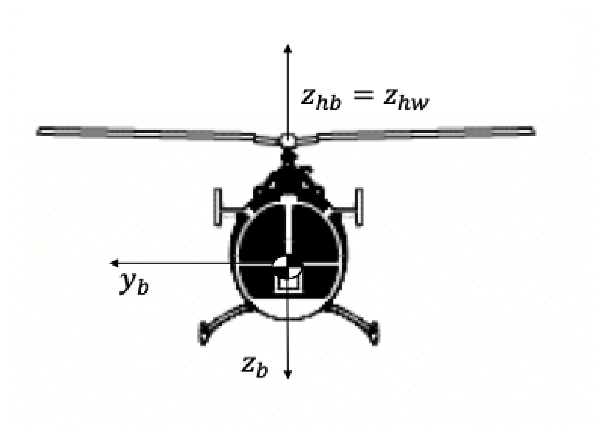

Figure 3: Helicopter yz view

1. Earth-fixed North-East-Down (NED) frame, $\mathbb{F}_E = \{O; \boldsymbol{x}_E, \boldsymbol{y}_E, \boldsymbol{z}_E\}$. This frame can be regarded as an inertial frame if the Earth is considered flat and not rotating. The origin is arbitrarily fixed to a point on Earth's surface. $\boldsymbol{x}_E$ points in the direction of geodetic North, $\boldsymbol{z}_E$ points downward along the Earth ellipsoid normal, and $\boldsymbol{y}_E$ completes the right-handed triad.

2. Rotor Hub-Wind frame $\mathbb{F}_{hw} = \{H; \boldsymbol{x}_{hw}, \boldsymbol{y}_{hw}, \boldsymbol{z}_{hw}\}$. Rotor forces and moments are computed using this frame. Its origin is the rotor hub. $\boldsymbol{z}_{hw}$ is aligned with the rotor shaft, downward. $\boldsymbol{x}_{hw}$, orthogonal to $\boldsymbol{z}_{hw}$, is aligned with the component of relative wind normal to the shaft axis. $\boldsymbol{y}_{hw}$ axis completes the right-handed orthogonal set.

3. Rotor Hub-Body frame $\mathbb{F}_{hb} = \{H; \boldsymbol{x}_{hb}, \boldsymbol{y}_{hb}, \boldsymbol{z}_{hb}\}$. $\boldsymbol{z}_{hb}$ axis is aligned with rotor shaft, pointing downward. This system coincides with the hub-wind system when the sideslip β_w is zero.

4. Body-Fixed frame $\mathbb{F}_b = \{P; \boldsymbol{x}_b, \boldsymbol{y}_b, \boldsymbol{z}_b\}$. Origin is at the centre of gravity of the rotorcraft. $\boldsymbol{x}_b$ axis is positive out of the nose of the rotorcraft in its plane of symmetry, $\boldsymbol{z}_b$ is perpendicular to $\boldsymbol{x}_b$ in the same plane of symmetry, pointing downward, and $\boldsymbol{y}_b$ axis completes the right-handed system. All forces and moments used in the body equations of motion are expressed relative to this system.

2.2. Equations of motion

Newton-Euler equations of motion in body reference frame $\mathbb{F}_b$ are used to describe aircraft dynamics:

(1) $$\dot{\boldsymbol{V}} = -\boldsymbol{\Omega} \times \boldsymbol{V} + \boldsymbol{F}^{(e)}/m$$

(2) $$\dot{\boldsymbol{\Omega}} = \boldsymbol{I}^{-1}[-\boldsymbol{\Omega} \times (\boldsymbol{I}\boldsymbol{\Omega}) + \boldsymbol{M}^{(e)}]$$

where m is the aircraft mass, $\boldsymbol{V} = [u, v, w]^T$ is the linear velocity vector, $\boldsymbol{\Omega} = [p, q, r]^T$ is the angular velocity vector, and $\boldsymbol{I}$ is the inertia tensor. $\boldsymbol{F}^{(e)}$ and $\boldsymbol{M}^{(e)}$ are the external forces and moments, respectively. Rigid-body kinematics is given by:

$$\begin{bmatrix}\dot{\phi}\\ \dot{\theta}\\ \dot{\psi}\end{bmatrix} = \begin{bmatrix}1 & \sin\phi\tan\theta & \cos\phi\tan\theta\\ 0 & \cos\phi & -\sin\phi\\ 0 & \sin\phi/\cos\theta & \cos\phi/\cos\theta\end{bmatrix}\boldsymbol{\Omega} \tag{3}$$

$$\begin{bmatrix}\dot{x}\\ \dot{y}\\ \dot{z}\end{bmatrix} = \Pi_{be}^{-1}\begin{bmatrix}u\\ v\\ w\end{bmatrix} \tag{4}$$

provided

$$\Pi_{be}^{-1} = \begin{bmatrix}c\theta c\psi & s\phi s\theta c\psi - c\phi s\psi & c\phi s\theta c\psi + s\phi s\psi\\ c\theta s\psi & s\phi s\theta s\psi + c\phi c\psi & c\phi s\theta s\psi - s\phi c\psi\\ -s\theta & s\phi c\theta & c\phi c\theta\end{bmatrix} \tag{5}$$

obtained by means of a $3-2-1$ rotation sequence, where ϕ, θ,and ψ are roll, pitch and yaw attitude angles respectively, provided $c(\cdot) = \cos(\cdot)$ and $s(\cdot) = \sin(\cdot)$.

2.3. Forces and moments

The total moment vector just includes the aerodynamic effect $\boldsymbol{M}^{(a)}$, unlike the external force vector, which also includes gravity effects $\boldsymbol{F}^{(g)}$, whose expression is:

$$\boldsymbol{F}^{(g)} = \mathbb{T}_{be}\begin{bmatrix}0\\ 0\\ mg\end{bmatrix} = \begin{bmatrix}-mg\sin\theta\\ mg\sin\phi\cos\theta\\ mg\cos\phi\cos\psi\end{bmatrix} \tag{6}$$

where g is the gravity acceleration and $\mathbb{T}_{be}$ is the rotation matrix from $\mathbb{F}_E$ to $\mathbb{F}_b$. The contributions of all aircraft components are used to calculate aerodynamic effects:

$$\boldsymbol{F}^{(a)} = \boldsymbol{F}^{(MR)} + \boldsymbol{F}^{(FU)} + \boldsymbol{F}^{(VS)} + \boldsymbol{F}^{(HS)} + \boldsymbol{F}^{(TR)} \tag{7}$$

$$\boldsymbol{M}^{(a)} = \boldsymbol{M}^{(MR)} + \boldsymbol{M}^{(FU)} + \boldsymbol{M}^{(VS)} + \boldsymbol{M}^{(HS)} + \boldsymbol{M}^{(TR)} \tag{8}$$

where MR stays for main rotor, TR for tail rotor, VS and HS for vertical and horizontal stabilizer, FU for fuselage.

2.3.1. Main rotor model

The principal source of thrust in a helicopter is the main rotor, whose mathematical model is based on the Talbot work.[15] Some of the authors recently presented a Talbot-based model for an ultralight helicopter.[16] The hypotheses made to model the main rotor are:[15]

1. In bending and torsion blades are considered rigid;
2. Twisting of the blades is linear;
3. The angles of flapping and inflow are small;
4. To evaluate the flapping only effects due to angular acceleration $\dot{p}$ and $\dot{q}$, angular velocity p, q and the normal acceleration of the aircraft motion are considered;
5. Compressibility and stall effects are not considered;
6. Reversed flow region is not considered;
7. The inflow is uniform but calculated dynamic;
8. The tip loss factor is assumed to be 1;
9. Blade flapping is approximated by the first harmonic terms with time-varying coefficients, that is:

$$\beta(t) = a_0(t) - a_1(t)\cos\psi - b_1(t)\sin\psi \tag{9}$$

The analytical tip-path plane dynamic equations are:

$$\ddot{\bar{\boldsymbol{a}}} + \tilde{D}\dot{\bar{\boldsymbol{a}}} + \tilde{K}\bar{\boldsymbol{a}} = \tilde{\bar{\boldsymbol{f}}} \tag{10}$$

where $\boldsymbol{a} = (a_0 \quad a_1 \quad b_1)^T$ and expressions for $\tilde{D}$, $\tilde{K}$ and $\tilde{f}$ are the same as reported in[15] . In order to obtain blade forces, momentum theory is employed integrating analytically over the radius. Detailed expressions for the derivation of forces and moments are given in Ref.[15]

The rotor inflow ratio must be known in order to calculate thrust. Static and dynamic inflow models are the two primary subcategories. The Pitt-Peters dynamic inflow model has been applied[17] , in contrast to that one presented by Talbot[15] . In the wind-hub reference frame, the implemented induced uniform inflow model is:

$$\frac{d}{dt} = \begin{pmatrix}\lambda_0\\ \lambda_s\\ \lambda_c\end{pmatrix} = \Omega\mathbb{M}^{-1}(-(\mathbb{L}_1\mathbb{L}_2)^{-1}\begin{pmatrix}\lambda_0\\ \lambda_s\\ \lambda_c\end{pmatrix} + \boldsymbol{C}_{aero}) \tag{11}$$

with $\lambda_s = \lambda_c = 0$ is set to zero to account only for the uniform inflow component (λ_0). Expressions for the matrices $\boldsymbol{C}_{aero}$, $\mathbb{M}$, $\mathbb{L}_1, \mathbb{L}_2$ are reported in.[17] λ, the total inflow, is:

$$\lambda = \frac{w_H}{\Omega R} - \lambda_0 \tag{12}$$

where w_H is the vertical velocity component in the Hub-Wind reference frame, Ω the MR rotational speed and R the MR radius. The formula for the rotor-induced velocity at the disk is:

$$v_i = (\frac{w_H}{\Omega R} - \lambda)\Omega R \tag{13}$$

Chen goes into detail about the tip-path plane dynamic equations derivation in[18] .

2.3.2. Tail rotor model

Also the tail rotor is modelled as in reference.[15] Since flapping frequency is significantly higher than that one of the main rotor, flapping and tip-path plane dynamics are disregarded. A steady-state solution is taken into consideration after setting the first and second derivatives of the blade-flapping non-rotating coordinates to zero. This means that in the force equations $\dot{a_o} = \dot{a_1} = \dot{b_1} = 0$ and $\ddot{a_0} = \ddot{a_1} = \ddot{b_1} = 0$. Forces and moments expressions are detailed in Appendix D of reference.[15]

The inflow ratio of the tail rotor is static and uniform and it is a steady state solution of the Pitt-Peters model,[17] whose expression is:

$$\lambda_{TR} = \frac{-v_{TR}}{\omega_{TR} R_{TR}} - \frac{CT_{TR}}{2\sqrt{\mu_{TR}^2 + \lambda_{TR}^2}} \tag{14}$$

that should be solved with the Newton-Ralphson iterative procedure. v_{TR} and w_{TR} are the lateral and vertical components of the TR velocities. CT_{TR} is the TR thrust coefficient, R_{TR} the TR radius and μ_{TR} the TR advance ratio.

2.3.3. Fuselage

The fuselage forces and moments are evaluated as a function of the angle of attack α_{FU} and the sideslip angle β_{FU}, as presented in reference.[19] The main equations involved are:

$$\boldsymbol{V}_{FU} = \boldsymbol{V}_b + \boldsymbol{\omega}_b \times \boldsymbol{r}_{FU} \tag{15}$$

$$\alpha_{FU} = \arctan \frac{w_{FU}}{u_{FU}} \tag{16}$$

$$\beta_{FU} = \arcsin \frac{v_{FU}}{|\boldsymbol{V}_{FU}|} \tag{17}$$

$$D_{FU} = \frac{1}{2}\rho |\boldsymbol{V}_{FU}|^2 S_{ref} C_D(\alpha, \beta) \tag{18}$$

$$Y_{FU} = \frac{1}{2}\rho |\boldsymbol{V}_{FU}|^2 S_{ref} C_Y(\alpha, \beta) \tag{19}$$

$$L_{FU} = \frac{1}{2}\rho |\boldsymbol{V}_{FU}|^2 S_{ref} C_L(\alpha, \beta) \tag{20}$$

Where D_{FU}, Y_{FU} and L_{FU} are, respectively, the fuselage drag, lateral and vertical forces in the wind system of axes about the fuselage reference point. Forces and moments in the body-fixed reference frame are:

$$\boldsymbol{F}_{FU}^b = \begin{bmatrix} -c\alpha_{FU} c\beta_{FU} & -s\alpha_{FU} s\beta_{FU} & s\alpha_{FU} \\ -s\beta_{FU} & c\beta_{FU} & 0 \\ -s\alpha_{FU} c\beta_{FU} & -s\alpha_{FU} s\beta_{FU} & c\alpha_{FU} \end{bmatrix} \tag{21}$$

$$\boldsymbol{M}_{FU}^b = \boldsymbol{r}_{FU} \times \boldsymbol{F}_{FU}^b \tag{22}$$

where c stays for $\cos$ ans s fon $\sin$. $\boldsymbol{V}_{FU}$, u_{FU}, v_{FU}, w_{FU} are the fuselage velocity vector and its components. S_{ref} is the reference surface for aerodynamic calculation and C_D, C_Y, C_L the aerodynamic coeeficient that are function of angle of attack and sideslip angles. $\boldsymbol{r}_{FU}$ is the position of the fuselage pressure center with respect to the gravity center of the rotorcraft. Aerodynamic coefficients are obtained both from data given by Padfield in his book[1] , both from charts of the induced velocities presented in[20] , adapted for the BO105 helicopter.

2.3.4. Empennages

The modelling of the vertical and horizontal stabilizers follows the approach presented in[15] with aerodynamic data given in[1] . As for fuselage model, aerodynamic interactions between main rotor, tail rotor and empennages are considered, such as MR and TR downwashes, according to.[20]

3. SLIDING MODE CONTROL THEORY OVERVIEW

Consider a multi-input multi-output (MIMO) linear system with multiple inputs and outputs that are impacted by matched uncertainty as follows:

$$\dot{x} = Ax + B\left(u + d\left(x, t\right)\right) \tag{23}$$
$$y = Cx \tag{24}$$

where $x \in R^n$ is the state vector, $u \in R^m$ is the control input vector, $y \in R^p$ is the output vector, $A \in R^{n \times n}$, $B \in R^{n \times m}$ and $C \in R^{p \times m}$. Referring to the works of,[11] the SMC strategy implemented in this paper includes an integral action. To implement such SMC it is necessary to augment the state with the error state resulting in the following augmented state vector $\bar{x} = [x_e, x]^{\mathbb{T}}$. The augmented system is described by the following $\bar{A}$ and $\bar{B}$ matrices:

$$\bar{A} = \begin{bmatrix} 0 & C \\ 0 & A \end{bmatrix}; \bar{B} = \begin{bmatrix} 0 \\ B \end{bmatrix} \tag{25}$$

The sliding control surface is defined as follows:

$$\mathcal{S} = \left\{ \bar{X} \in \mathbb{R}^{p+n} : \sigma\left(\bar{x}\right) = 0 \right\} \tag{26}$$

σ is calculated by multiplying the design matrix S with $\bar{x}$. The matrix S is a real matrix with dimensions of m by $(n+p)$, and it describes the state dynamics that occur during the induced sliding motion. Defining the matrix $\bar{T} = [I_p, 0_{n\times p}]^{\mathbb{T}}$ it is finally possible to write the complete augmented dynamic system equations as follows:

$$\dot{\bar{x}} = \bar{A}\bar{x} + \bar{B}\left(u+d\right) - \bar{T}r \tag{27}$$

To maintain the progression of system states on the sliding motion surface, the system must fulfill the following requirements:

$$\dot{\sigma} = \Phi\sigma - \rho\text{sign}\left(\sigma\right) + SBd \tag{28}$$

The formula consists of a design matrix represented by the symbol Σ, a tuning parameter indicated by ρ, and the non-continuous sign function **sign**(σ). The purpose of the non-continuous function is to counterbalance any disturbances or uncertainties represented through the term Bd. If the system states do not evolve according to the desired dynamics, specifically the sliding surface, then the product of ρsign (sign) will not be zero, and the control system will be able to compensate for the uncertainties and disturbances. A control law is developed taking into account the Lyapunov function:

$$V\left(\sigma\right) = \sigma^{\mathbb{T}}P\sigma \tag{29}$$

The Lyapunof function derivative is as follows:

$$\dot{V} = \sigma^{\mathbb{T}}\left(\Phi^{\mathbb{T}}P + P\Phi\right)\sigma + 2\sigma^{\mathbb{T}}P\alpha \tag{30}$$

$$\alpha = SBd - \rho\text{sign}\left(\sigma\right) \tag{31}$$

For system stability, choose P as the solution for the Lyapunov equation $\Phi^{\mathbb{T}}P + P\Phi = -I$, where I is the identity matrix. To meet this requirement, ensure that α is negative and ρ is greater than or equal to $||SB|| + \gamma$, where γ is a design parameter.

To obtain the control law, we start by considering that σ equals the product of S and $\bar{x}$, and its derivative is equal to $S\dot{\bar{x}}$. We can use the following equation:

$$S\left(\bar{A}\bar{x} + \bar{B}\left(u+d\right) - \bar{T}r\right) = \Phi\sigma + \alpha \tag{32}$$

By performing some algebraic operations on (32), we can derive the expression of the control law, which is:

$$u = -\left(S\bar{B}\right)^{-1}\left(S\bar{A} - \Phi S + \bar{T}r - \rho\text{sign}\left(\sigma\right)\right) \tag{33}$$

Functions like the sign can create chattering in the system. Chattering occurs when the control action switches continuously between different modes or control laws. This rapid switching can cause high-frequency oscillations in the control signal, resulting in undesired and noisy behavior in the controlled system. This behavior can also lead to unnecessary wear and tear on actuators, reducing their lifespan. Furthermore, it can cause unwanted vibrations and noise in the controlled system, impacting its overall performance and stability. In this work, in order to mitigate chattering, we have used the following sigmoidal transition function:

$$\Sigma\left(\sigma\right) = \frac{\sigma}{|\sigma| + \epsilon} \tag{34}$$

In equation (34), the sigmoid function gradually transitions from one value to another, which helps avoid abrupt changes. This function helps to make the control action near the sliding surface smoother, ultimately reducing chattering and its negative consequences.

4. CONTROL SYSTEM ARCHITECTURE

4.1. General architecture

A hierarchical control system architecture is a commonly used design approach in managing and controlling complex systems. Our design involves two levels or layers of control; the inner level is responsible for attitude control and consists of two sub-layers, a proportional control (P) that controls attitude itself and provides reference angular speed to the second layer, which consists of an angular speeds controller which is a proportional-integral controller (PI). The outer loop is speed control, which includes a SMC for horizontal and lateral speed and an $\mathcal{L}_1$ control for vertical speed. This architecture promotes efficiency and scalability, making managing a complex system like a helicopter easier. The control architecture is shown in Figure 4, while Figure 5 provides a more detailed view of the cascaded P-PI control architecture. SMC outputs pitch and roll reference angles tracked by the internal layer. The internal layer directly receives the yaw reference from the pilot. The decision to use an SMC controller to regulate horizontal and lateral speed arises from the fastness and robustness of this kind of control algorithm. The vertical speed outer loop control consists of an adaptive $\mathcal{L}_1$ controller with an architecture analogous to those in the references[9].[10] Using an adaptive controller to generate the collective control ensures a robust tracking of the helicopter's vertical speed despite external disturbances and decoupling from the other axis.

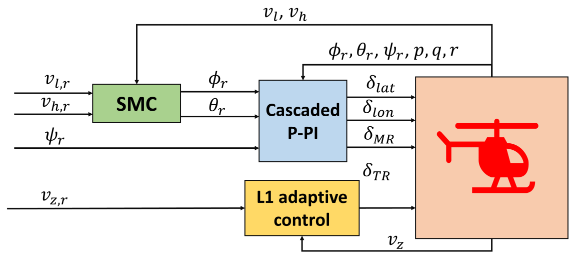

Figure 4: Control system architecture main scheme

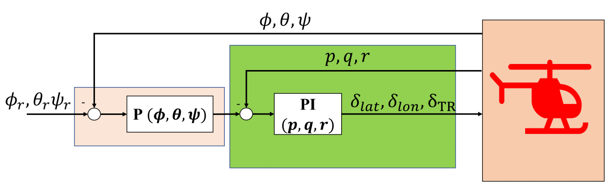

Figure 5: P-PI cascaded inner control loop

4.2. SMC implementation

The SMC generates pitch and roll references for the inner loop. To this purpose, the following sliding surfaces σ are chosen:

$$\sigma = \begin{bmatrix} v_l + \lambda_l \int_0^t (v_l - v_{lr})\, d\tau \\ v_h + \lambda_h \int_0^t (v_h - v_{hr})\, d\tau \end{bmatrix} \tag{35}$$

Such sliding surfaces describe the desired horizontal and lateral speed dynamics that we would like the helicopter to follow.

Lateral acceleration a_l and horizontal acceleration a_h are described by the following equations:

$$\begin{pmatrix} a_l \\ a_h \end{pmatrix} = \begin{bmatrix} \frac{g}{cos(\theta)} & 0 \\ gtan\,(\theta)\, tan\,(\phi) & -g \end{bmatrix} \begin{pmatrix} \Delta\phi \\ \Delta\theta \end{pmatrix} \tag{36}$$

which can be rewritten as:

$$\begin{pmatrix} \dot{v}_l \\ \dot{v}_h \end{pmatrix} = G \begin{pmatrix} \Delta\phi \\ \Delta\theta \end{pmatrix} \tag{37}$$

The matrices $\bar{A}$, $\bar{B}$, $\bar{T}$ and S are as follows:

$$\bar{A} = \begin{bmatrix} 0_{2\times2} & I_2 \\ 0_{2\times2} & 0_{2\times2} \end{bmatrix}; \bar{B} = \begin{bmatrix} 0_{2\times2} \\ G \end{bmatrix}$$
$$\bar{T} = \begin{bmatrix} I_2 \\ 0_{2\times2} \end{bmatrix}$$

The control input is computed as in the equation (33).

5. SIMULATION RESULTS

The nonlinear aircraft model described in Section 2, characterized by BO105 helicopter mass and inertia properties, and geometric and aerodynamic data, listed in Appendix A, is implemented in the Matlab/Simulink environment. In order to assess the goodness of the control system, the proposed architecture has been tested in three maneuvers, namely the bob-down and bob-up maneuver, the slalom maneuver, and a rectangular-shaped trajectory. The maneuvers are chosen in accordance with the well-established military standard[21] , which outlines the rotorcraft response qualities needed to carry out a variety of tasks. The main goal is to evaluate helicopter performance.

In all three scenarios examined in this paper, the intended maneuver is executed both in the absence and in presence of wind disturbances, that are described in detail in[9] . This disturbance is directly included in the helicopter model as additional components of velocities and rates in body reference frame. For the sake of completeness, wind speed profiles and wind rates profiles are reported in Figures 6, 7.

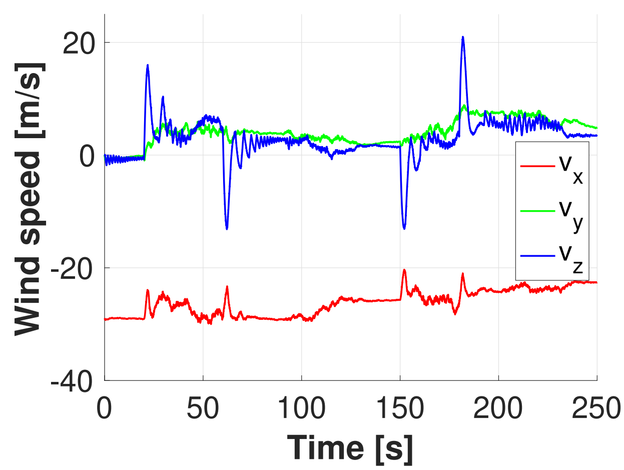

Figure 6: Wind speed components

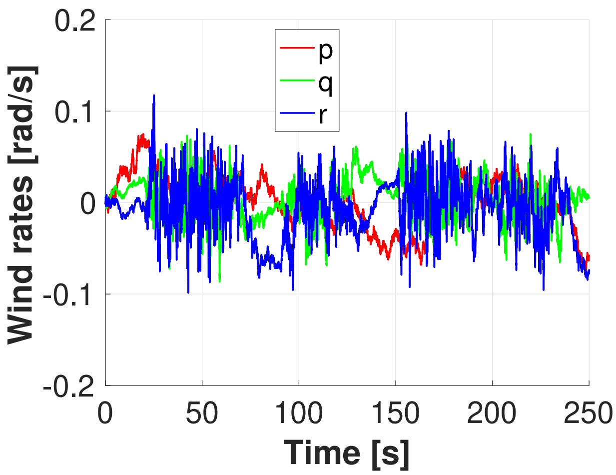

Figure 7: Wind rates components

These figures show the result of the combined implementation of three wind models: the discrete wind gust, the shear wind and the Dryden turbulence,[22].[23] The discrete wind gust implements a wind gust of the standard one minus cosine shape. The gust velocity is represented by:

$$V_{\text{wind}} = \begin{cases} 0 & x < 0 \\ \frac{V_m}{2}(1 - \cos\frac{\pi x}{d_m}) & 0 \leq x \leq d_m \\ V_m & x > d_m \end{cases} \tag{38}$$

where V_m is the gust amplitude, d_m the gust length, x the distance traveled and V_{wind} is the resultant velocity in the body axis frame. The magnitude of the mean shear wind profile is a function of altitude and the measured wind speed at 6 m above the ground:

$$u_w = W_{20}\frac{\ln\frac{h}{z_0}}{\ln\frac{20}{z_0}} \quad 3ft < h < 1000ft \tag{39}$$

where u_w is the mean wind speed, W_{20} is the measured wind speed at an altitude of 6 m, h is the altitude and z_0 is a constant dependent on the flight phase. The Dryden wind turbulence model adds atmospheric turbulence by using band-limited white noise with appropriate digital filter finite difference equations.

5.1. Bob-down and Bob-up maneuver

The bob-down and bob-up maneuver is presented as first, being very frequently used during the preliminary flight test. It is a simple combination of vertical and horizontal flight path segments. It starts with the helicopter being in hovering at approx. 610 m with heading angle pointing North with a zero value. Then it is accelerated to forward speed of 15 m/s at a constant altitude for 20 s and then it is decelerated back to hover. After that, the helicopter is commanded to descent for 10 s at a constant rate of 5 m/s, followed again by hover at a lower altitude. It is then accelerated again to 15 m/s for 20 s and decelerated again to hover and then it is asked to climb for 10 s at 5 m/s. Finally, it is asked to hover approximately at the initial altitude. During the entire maneuver, lateral velocity v_l and heading angle ψ are fixed to zero. Figure 8 displays the maneuver trajectory in presence and in absence of wind, showing a small deviation of the trajectory when wind disturbance is added.

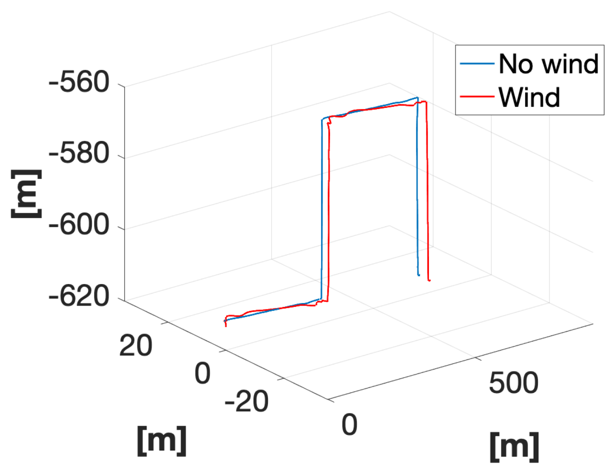

Figure 8: Trajectory in bob-down and bob-up maneuver

Based on Figures 9 and 10, it is evident that the heave axis dynamics are satisfactory, regardless of the presence or absence of wind. The vertical speed is accurately tracked, and the couplings with the other axes are minimal. Indeed the $\mathcal{L}_1$ adaptive controller can effectively mitigate disturbance and uncertainty despite its simple architecture. Horizontal and lateral velocities are controlled using the proposed architecture's tracking performance is shown in Figures 11 and 12, demonstrating its ability to navigate both with and without wind disturbances using a sliding mode controller. In the absence and presence of wind, Figures 13 and 14 display the heading angle tracking. A P-PI controller with a single set of parameters for the entire flight envelope controls the heading angle. Although couplings with other axes and wind effects are insignificant, they are present, as shown in the figures. During all the maneuver, the heading error is maintained lower than 5 deg, that accordingly to[21] , is satisfactory for a helicopter during hover and vertical maneuvers.

Commands for the helicopter, computed by the proposed hierarchical architecture, both in the presence and absence of wind, can be found in Figures 15 and 16.

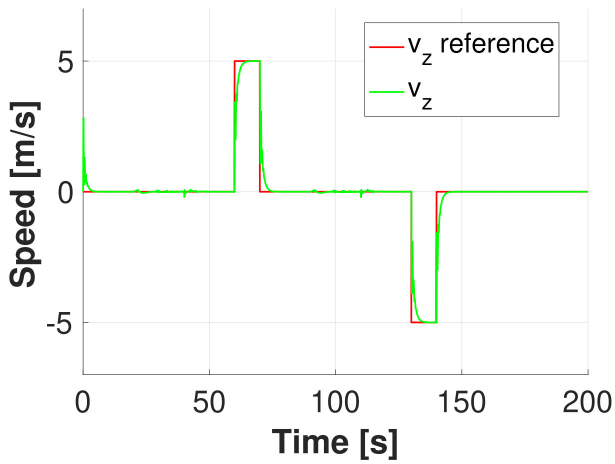

Figure 9: Vertical speed in bob-down and bob-up maneuver

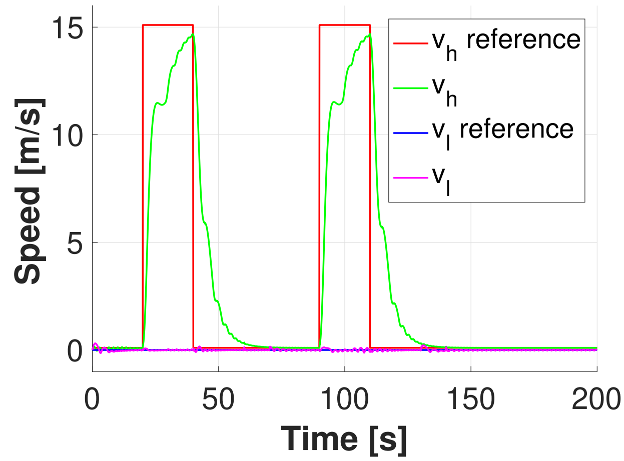

Figure 11: Horizontal and lateral speed in bob-down and bob-up maneuver

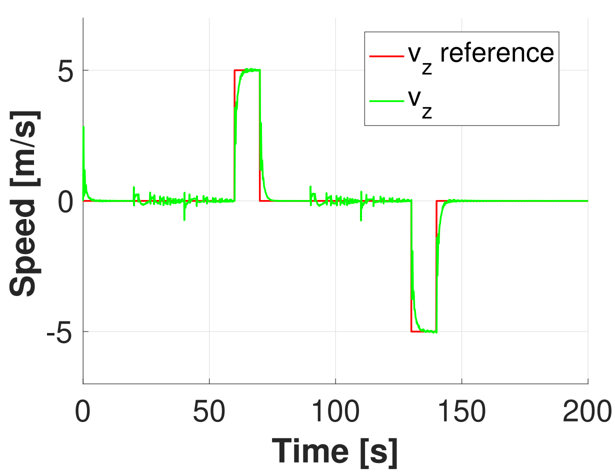

Figure 10: Vertical speed in bob-down and bob-up maneuver with wind disturbance

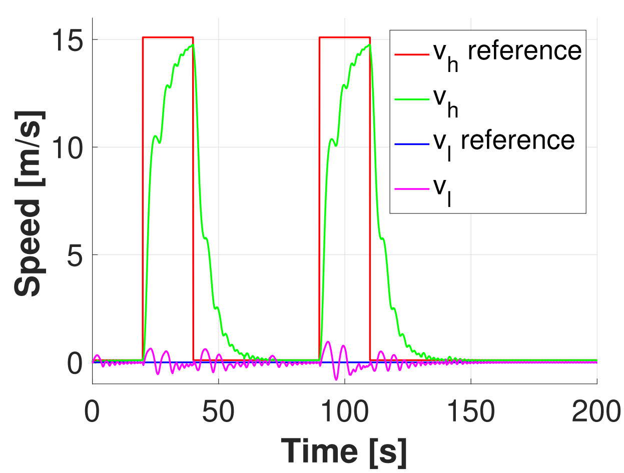

Figure 12: Horizontal and lateral speed in bob-down and bob-up maneuver with wind disturbance

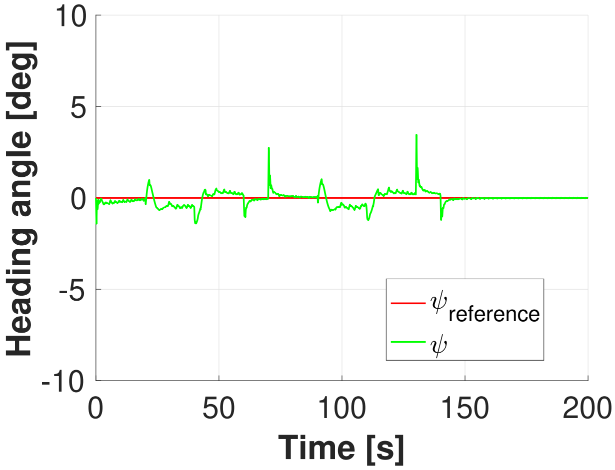

Figure 13: Heading angle in bob-down and bob-up maneuver

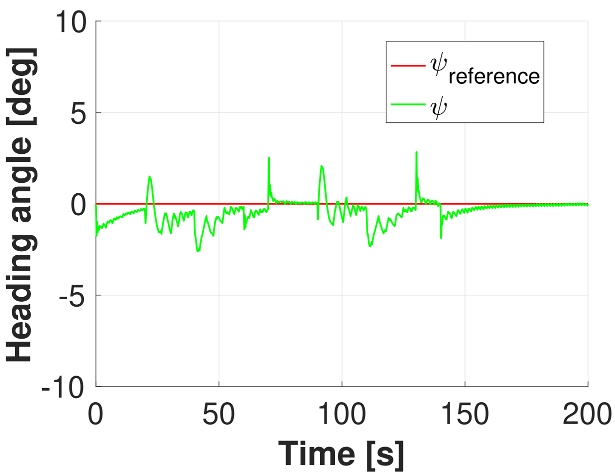

Figure 14: Heading angle in bob-down and bob-up maneuver with wind disturbance

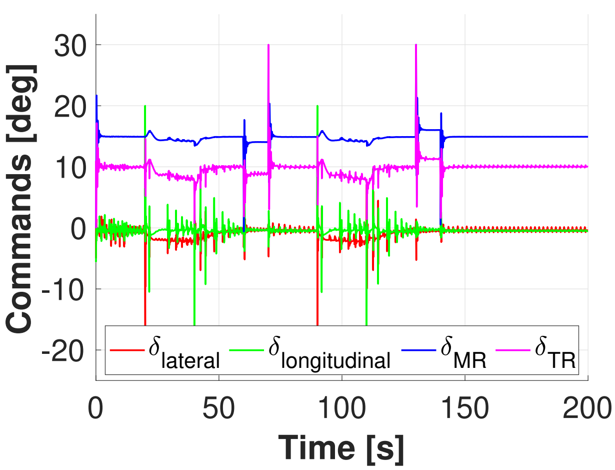

Figure 15: Commands in bob-down and bob-up maneuver

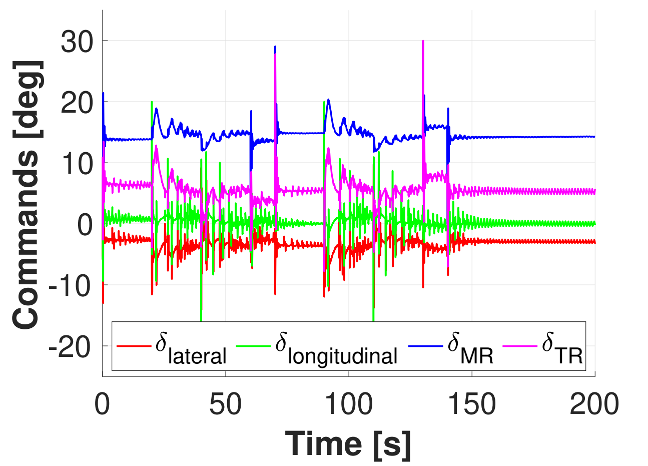

Figure 16: Commands in bob-down and bob-up maneuver with wind disturbance

5.2. Slalom maneuver

The slalom maneuver is a more challenging test. The primary purpose of flying the designed architecture using this maneuver is to test the controller's ability to maintain precise control and maneuverability while flying at constant altitudes in confined spaces, such as urban areas or mountainous terrain. Practically, the maneuver is initiated with the helicopter hovering with a zero heading angle at a constant altitude. Then, a doublet is commanded to the lateral velocity v_l with an amplitude of 5 m/s and a duration of 20 s respectively. The slalom maneuver trajectory both in the absence and in the presence of wind is shown in figure 17.

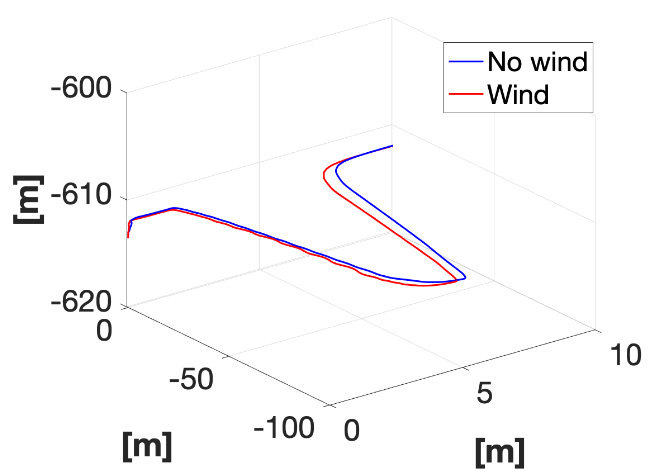

Figure 17: Trajectory in slalom maneuver

Figures 18 and 19 display the horizontal and lateral speed during the slalom maneuver in both still and windy conditions. The SMC controller effectively tracks the reference and any coupling between the two axes are negligible. These results demonstrate the controller's reliable performance.

Vertical speed tracking of the $\mathcal{L}_1$ adaptive control is shown in Figures 22 and 23 in the absence and in the presence of wind respectively. Also in this case the controller is able of reject disturbances and is almost insensitive to couplings with the other axis.

Figures 22 and 23 show the heading angle as tracked by the P-PI controller in the absence and in the presence of wind respectively. The heading angle performances are satisfactory and the wind disturbance is rejected. Decoupling effects are also negligible.

In this maneuver, the helicopter commands are depicted in Figures 24 and 21. These figures illustrate the commands when the helicopter is not impacted by wind disturbances and when it is affected by them.

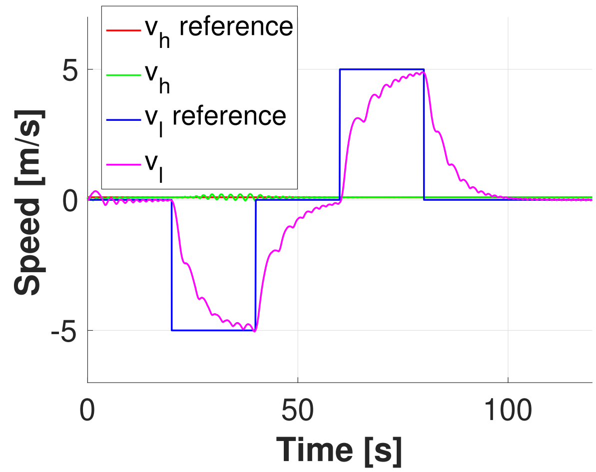

Figure 19: Horizontal and lateral speed in slalom maneuver with wind disturbance

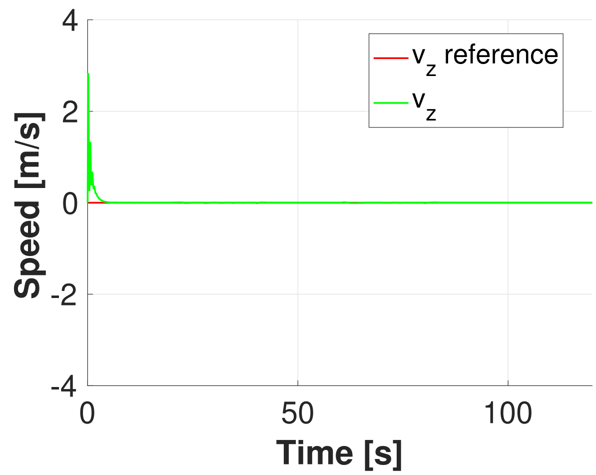

Figure 20: Vertical speed in slalom maneuver

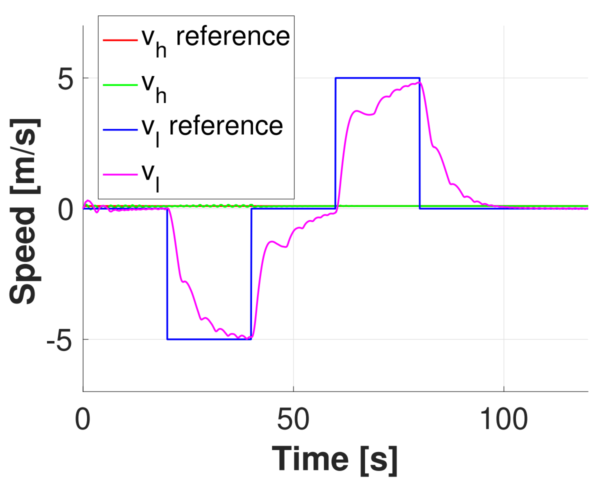

Figure 18: Horizontal and lateral speed in slalom maneuver

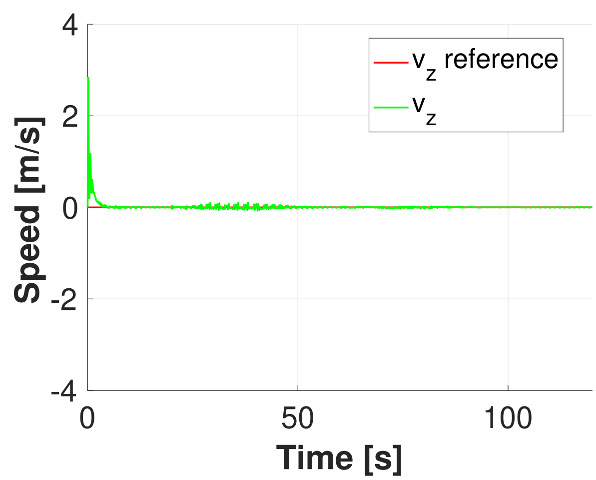

Figure 21: Vertical speed in slalom with wind disturbance

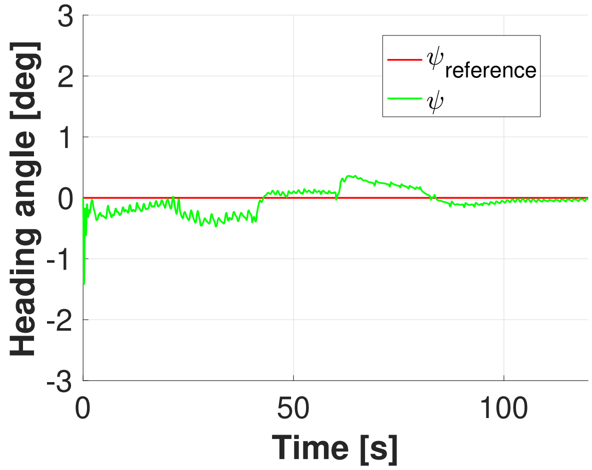

Figure 22: Heading angle in slalom maneuver

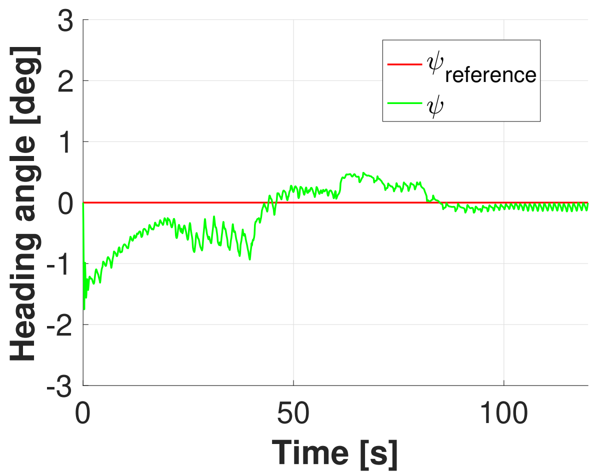

Figure 23: Heading angle in slalom maneuver with wind disturbance

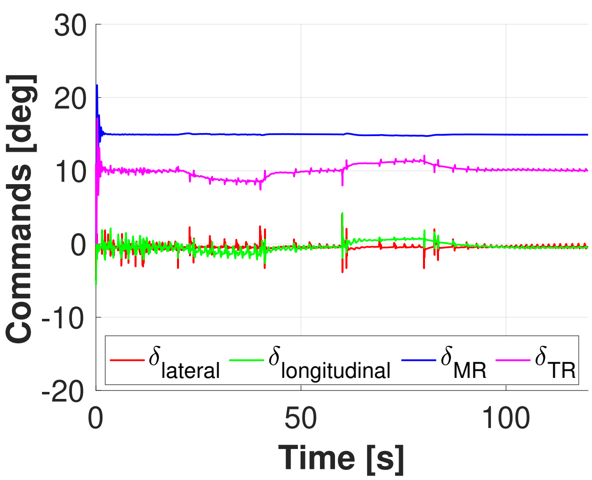

Figure 24: Commands in slalom maneuver

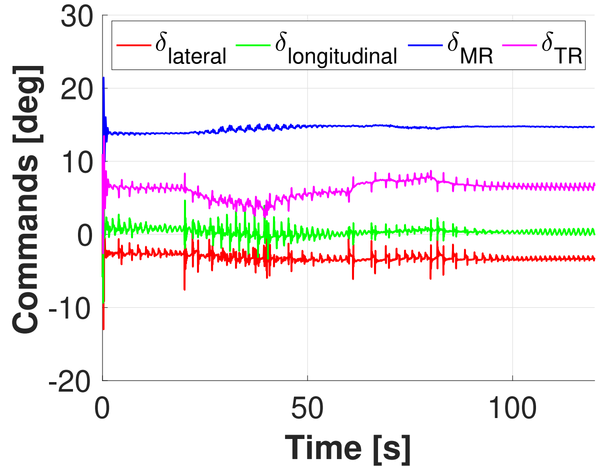

Figure 25: Commands in slalom maneuver with wind disturbance

5.3. Rectangular maneuver

The final test for the proposed control architecture is a maneuver where the helicopter is required to move in a closed, rectangular loop while maintaining a consistent heading and altitude. The only way to move is by adjusting the horizontal and lateral speed, allowing for testing of the coupling between the yaw and vertical axis and the longitudinal vertical axis. The helicopter starts this maneuver in hovering at a constant altitude. Firts, it is accelerated for 40 s at 25 m/s, back to hover and then it is asked to keep a positive lateral velocity of 10 m/s for 30 s. The helicopter is again keeped in hovering and the decelerated for 40 s to -30 m/s and then it has to mantain for 30 s a negative lateral velocity of -10 m/s. Finally it is decelerated to hovering, approximately at the starting point. All the maneuver is done with constant altitude and heading angle. Figure 26 shows the square maneuver in presence and in absence of wind disturbance.

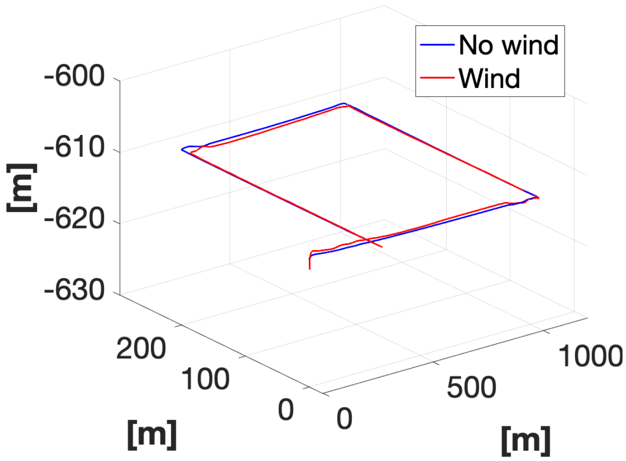

Figure 26: Trajectory in square maneuver

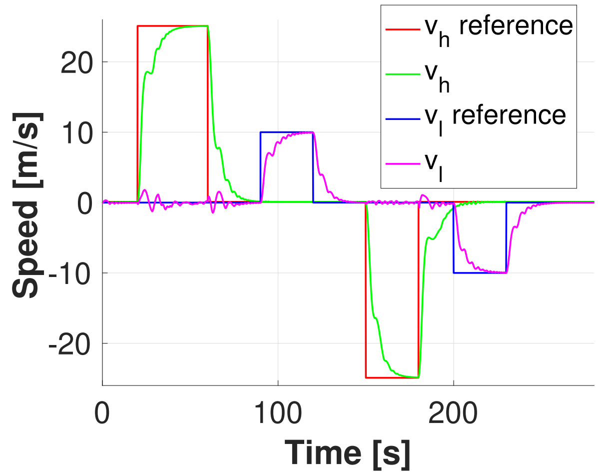

Figure 28: Horizontal and lateral speed in square maneuver with wind disturbance

Similar considerations made for the two previous cases can be made also for the rectangular maneuver. Longitudinal, lateral, and vertical speed shows satisfactory performances, achieves disturbance rejection, and an effective axis decoupling. Figures 27, 29, 28, 29 show the longitudinal, lateral, and vertical speed in the absence and in the presence of wind.

Also with this maneuver, the heading angle P-PI controller shows satisfactory performances as Figures 31 and 32 prove.

Also in this test simulation test case the commands are in Figures 34 and 33.

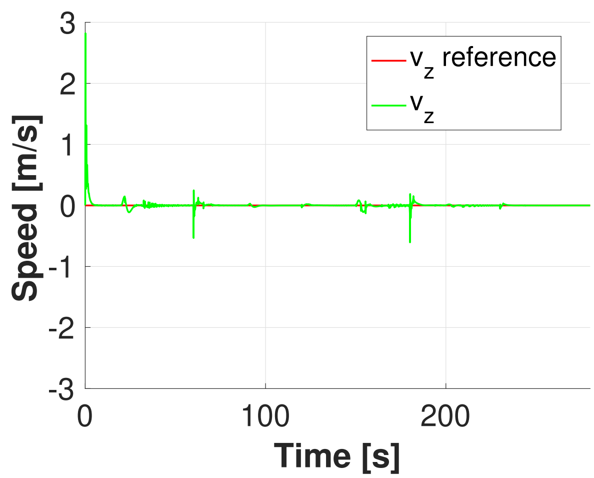

Figure 29: Vertical speed in square maneuver

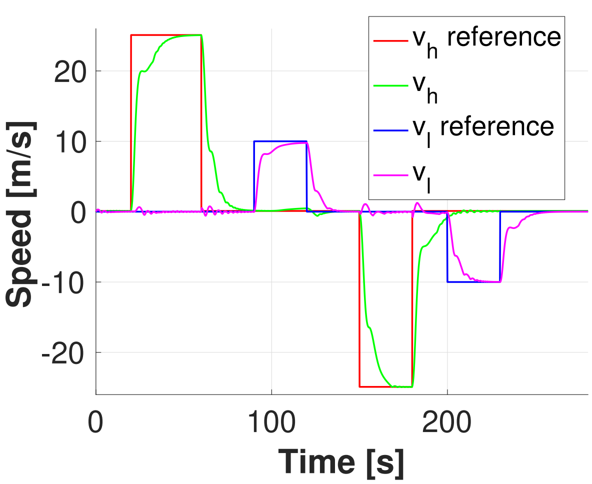

Figure 27: Horizontal and lateral speed in square maneuver

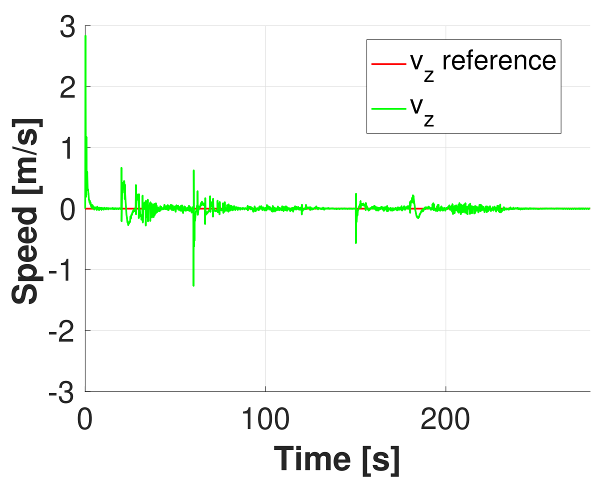

Figure 30: Vertical speed in square with wind disturbance

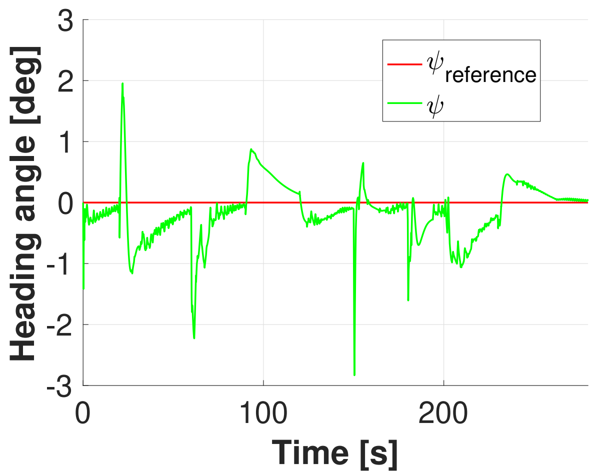

Figure 31: Heading angle in square maneuver

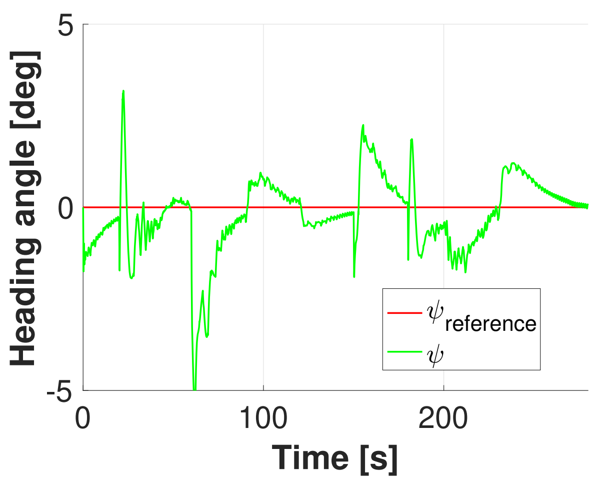

Figure 32: Heading angle in square maneuver with wind disturbance

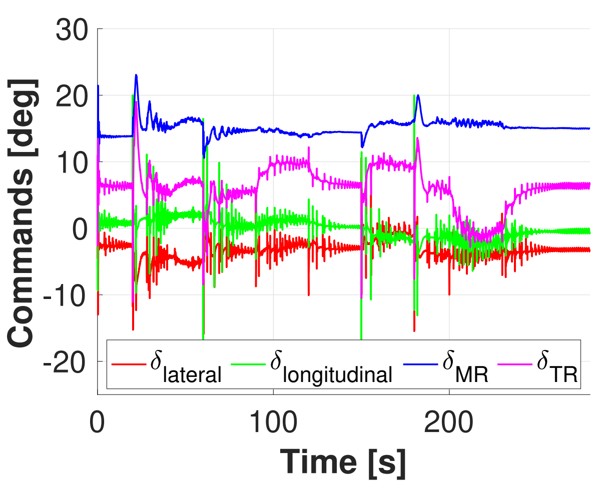

Figure 33: Commands in square maneuver with wind disturbance

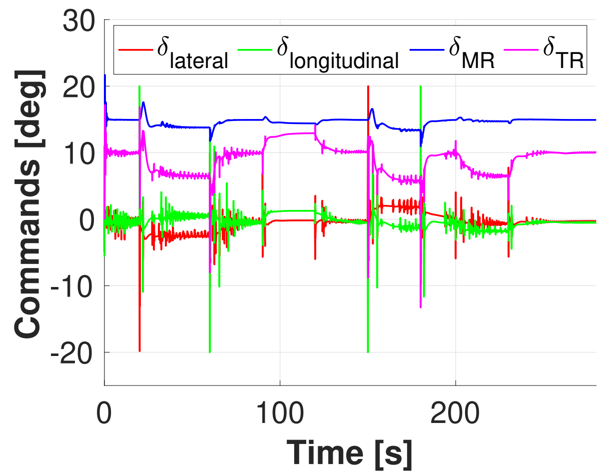

Figure 34: Commands in square maneuver

6. CONCLUSIONS

In this work, a hierarchical combined control strategy is tested through simulation, which involves performing three key test maneuvers for a helicopter. While this work may be considered preliminary, it demonstrates that various control algorithms can effectively be combined to operate satisfactory a helicopter.

COPYRIGHT STATEMENT

ACKNOWLEDGEMENTS

This study was carried out within the MOST - Sustainable Mobility National Research Center and received funding from the European Union Next-GenerationEU (PIANO NAZIONALE DI RIPRESA E RESILIENZA (PNRR) - MISSIONE 4 COMPONENTE 2, INVESTIMENTO 1.4 - D.D. 1033 17/06/2022, CN00000023). This manuscript reflects only the authors' views and opinions, neither the European Union nor the European Commission can be considered responsible for them.

APPENDIX A

Table 1: Helicopter relevant parameters.

Parameter	**Symbol**	**Value**	**Units**
Vehicle data			
Mass	m	2200	kg
Center of gravity stationline	STA_{CG}	2.1337	m
Center of gravity buttline	BL_{CG}	0	m
Center of gravity waterline	WL_{CG}	1.52	m
Moment of inertia	$I_x,\ I_y,\ I_z$	1433, 4973, 4099	kg m^2
Inertia products	$I_{xy},\ I_{yz},\ I_{xz}$	0, 0, 660	kg m^2
Main Rotor			
Number of blades	N_b	4	-
Radius	R_{MR}	4.91	m
Chord	c_{MR}	0.27	m
Rotational speed	Ω_{MR}	423.9918	rpm
Hinge offset	ε	0	m
Flapping spring constant	K_β	113330	N m/rad
Tangent of δ_3	K_1	0	-
Blade twist	θ_{tMR}	-0.14	rad
Precone angle	a_{0MR}	0	rad
Solidity	σ_{MR}	0.07	-
Lift curve slope	a_{MR}	6.113	1/rad
Blade inertia moment	I_β	231.7	kg m^2
MR hub stationline	STA_H	2.1337	m
MR hub buttline	BL_H	0	m
MR hub waterline	WL_H	3	m
Tail Rotor			
Number of blades	N_b	2	-
Radius	R_{TR}	0.95	m
Chord	c_{TR}	0.1791	m
Rotational speed	Ω_{TR}	2227.7	rpm
Tangent of δ_3	K_{1TR}	-1	-
Blade twist	θ_{tMR}	0	rad
Solidity	σ_{TR}	0.12	-
Lift curve slope	a_{TR}	5.7	1/rad
Blade inertia moment	I_β	0.6367	kg m^2
TR hub stationline	STA_{TR}	8.1337	m
TR hub buttline	BL_{TR}	-0.5	m
TR hub waterline	WL_{TR}	3.24	m
Fuselage			
Fus. aerodynamic ref. point stationline	STA_{FUS}	2.15	m
Fus. aerodynamic ref. point buttline	BL_{FUS}	0	m
Fus. aerodynamic ref. point waterline	WL_{FUS}	1.52	m
Plan area	S_{front}	7.4263	m^2
Side area	S_{lat}	5.2	m^2
Horizontal stabilizer (HS)			
HS. aerodynamic ref. point stationline	STA_{FUS}	6.6937	m
HS. aerodynamic ref. point buttline	BL_{FUS}	0	m
HS. aerodynamic ref. point waterline	WL_{FUS}	2	m
HS. area	$Area_{HS}$	0.803	m^2
HS. aero chord	c_{HS}	0.674	m
HS. aspect ratio	AR_{HS}	2.635	-
HS. incidence angle	α_{HS}	0.0698	rad
Vertical stabilizer (VS)			
VS. aerodynamic ref. point stationline	STA_{VS}	7.5497	m
VS. aerodynamic ref. point buttline	BL_{VS}	0	m
VS. aerodynamic ref. point waterline	WL_{VS}	2.5	m
VS. area	$Area_{VS}$	0.805	m^2
VS. aero chord	c_{VS}	0.5358	m
VS. dynamic pressure ratio	AR_{VS}	0.41	-
VS. incidence angle	α_{VS}	-0.08116	rad

References

[1] Padfield, G. D., Helicopter Flight Dynamics, 1st ed., John Wiley and Sons, Ltd, 2007

[2] Muchiri, G. N., and S. Kimathi., A review of applications and potential applications of UAV. - Proceedings of the Sustainable Research and Innovation Conference. 2022. p. 280-283.

[3] de Angelis, E.L., Giulietti, F., Dynamic stability and control of rotorcraft for suspended load transportation: an analytical approach. - European Rotorcraft Forum 2022, Winterthur, paper No.94, 2022.

[4] Postlethwaite, I., Smerlas, A., Walker, D. J., Gubbels, A. W., Baillie, S. W., Strange, M. E., and Howitt, J., H_∞ Control of the NRC Bell 205 Fly-by-Wire Helicopter, Journal of the American Helicopter Society, Vol. 44, No. 4, 1999, pp. 276-284.

[5] Smerlas, A. J., Walker, D. J., Postlethwaite, I., Strange, M. E., Howitt, J., and Gubbels, A. W., Evaluating H_∞ Controllers on the NRC Bell 205 Fly-by-wire Helicopter, Control Engineering Practice, Vol. 9, No. 1, 2001, pp. 1-10.

[6] Ngo, T. D., and Sultan, C., Model Predictive Control for Helicopter Shipboard Operations in the Ship Airwakes, Journal of Guidance, Control, and Dynamics, Vol. 38, No. 12, 2015, pp. 574-589.

[7] C. Liu, W. H. Chen and J. Andrews, Model predictive control for autonomous helicopters with computational delay, UKACC International Conference on Control 2010, Coventry, 2010, pp. 1-6.

[8] Raaja G. S., Vinodh K. E., Robust MRAC augmented baseline LQR for tracking control of 2 DoF helicopter, Robotics and Autonomous Systems, Volume 86, 2016, Pages 70-77.

[9] Ryals, A.D., Bertolani, G., Pollini, L., Giulietti, F., $\mathcal{L}_1$ adaptive attitude augmentation of a small scale unmanned helicopter - Proceedings of the 2023 International Conference on Unmanned Aircraft Systems (ICUAS), p. 1081-1088. DOI 10.1109/ICUAS57906.2023.10156363

[10] Ryals, A.D., Bertolani, G., Pollini, L., Giulietti, F., $\mathcal{L}_1$ adaptive speed control for a helicopter, Proceedings of the 48rd European Rotorcraft Forum, ERF 2022, Winterthur 6-8 September 2022

[11] Halbe, O., Hajek, M. (2020). Robust Helicopter Sliding Mode Control for Enhanced Handling and Trajectory Following. Journal of Guidance, Control, and Dynamics.

[12] Halbe O, Hajek M., A Continuous Multivariable Finite-Time Super-Twisting Attitude and Rate Controller for Improved Rotorcraft Handling. Aerospace. 2022;

[13] McGeoch, D., McGookin, E., Houston, S., MIMO Sliding Mode Attitude Command Flight Control System for a Helicopter. AIAA Guidance, Navigation, and Control Conference and Exhibit, AIAA Paper 2005-6350.

[14] Bichlmeier, M., Holzapfel, F., Xargay, E., Hovakimyan, N. (2013). L1 Adaptive Augmentation of a Helicopter Baseline Controller.

[15] Talbot, P.D., Tinling, B.E., Decker, W.A., Chen, R.T.N., A mathematical model for a single main rotor helicopter for piloted simulation- Ames Reasearch Center, Moffett, Field, California, Sept. 1982

[16] de Angelis, E.L., Giulietti, F., Rossetti, G., Turci, M., Albertazzi, C., Toward smart air mobility: control system design and experimental validation for an unmanned light helicopter - Drones, MDPI, 7, 288, May 2023, https://doi.org/10.3390/drones7050288

[17] Peters, D. A., HaQuang, N., Dynamic inflow for practical applications - Journal of the American Helicopter Society, Vol.33, No.4, pp. 64-68, 1988, doi.org/10.4050/JAHS.33.64

[18] Chen, R.T.N., A simplified rotor system mathematical model for piloted flight dynamics simulation - Ames Reasearch Center, Moffett, Field, California, May 1979

[19] Heffley, R.K., Mnich, M.A., Minimum complexity helicopter simulation math model - Ames Reasearch Center, Moffett, Field, California, April 1988

[20] Jewel, J.W., Heyson, H.H., Charts of the induced velocities near a lifting rotor - NASA Memorandum 4-15-59L, Langley research center, Langley Field, Va, May 1959

[21] United States Army, Aviation and Missile Command., Aeronautical design standard, performance specification and handling qualities requirements for military rotorcraft, March 2000

[22] Military specification: Flying qualities of piloted airplanes mil-f-8785c, Force, US Air, 1980

[23] U.S. military handbook MIL-HDBK-1797B, Force, US Air, 2012